



Influence of the Xianshuihe Fault Zone on *In-Situ* Stress Field of a Deep Tunnel and its Engineering Effect

Dong Yuan^{1,2,3}, Lanbin Zhang^{1,2*}, Xiaoling Liu^{1,2*}, Tao Feng³, Guangze Zhang³, Zhengxuan Xu³, Zhewei Wang³, Xiaojuan Yi³, Zhiheng Lin³, Yang Ren⁴, Ru Zhang^{1,2} and Li Ren^{1,2}

¹State Key Laboratory of Hydraulics and Mountain River Engineering, College of Water Resource and Hydropower, Sichuan University, Chengdu, China, ²MOE Key Laboratory of Deep Earth Science and Engineering, Sichuan University, Chengdu, China, ³China Railway Eryuan Engineering Group Company, Ltd., Chengdu, China, ⁴State Key Lab Geohazard Prevent and Geoenvironm Pro, Chengdu University of Technology, Chengdu, China

OPEN ACCESS

Edited by:

Guang-Liang Feng,
Institute of Rock and Soil Mechanics
(CAS), China

Reviewed by:

Shikuo Chen,
Southwest Jiaotong University, China
Changbao Guo,
Chinese Academy of Geological
Sciences (CAGS), China

*Correspondence:

Lanbin Zhang
2021223060011@stu.scu.edu.cn
Xiaoling Liu
Dazzling_Liu@163.com

Specialty section:

This article was submitted to
Geohazards and Georisks,
a section of the journal
Frontiers in Earth Science

Received: 01 March 2022

Accepted: 06 April 2022

Published: 28 April 2022

Citation:

Yuan D, Zhang L, Liu X, Feng T,
Zhang G, Xu Z, Wang Z, Yi X, Lin Z,
Ren Y, Zhang R and Ren L (2022)
Influence of the Xianshuihe Fault Zone
on *In-Situ* Stress Field of a Deep Tunnel
and its Engineering Effect.
Front. Earth Sci. 10:886876.
doi: 10.3389/feart.2022.886876

The *in-situ* stress distribution near a fault zone is affected by factors such as tectonic movement and rock mass property deterioration, and it often shows unique characteristics and further affects the mechanical response of the rock mass and the safety of underground engineering construction. The Xianshuihe fault zone is one of the most active fault zones in the world. To understand the impact of the Xianshuihe fault zone on a tunnel under construction in southwestern China, the *in-situ* stress measured near the tunnel site at different distances from the faults of the Xianshuihe fault zone is obtained. Furthermore, the characteristics of the *in-situ* stress at the tunnel site and its engineering influence effect are analyzed. The results indicate the following: 1) Around the Xianshuihe fault zone, the fault mainly affects the maximum horizontal principal stress and the minimum horizontal principal stress in the shallow strata, and the *in-situ* stress closer to the fault is more greatly affected. 2) In the shallow area near the Selaha-Kangding fault, the maximum horizontal principal stress, minimum horizontal principal stress and lateral pressure coefficient at a borehole increase with increasing distance from the fault. Greater than 600 m from the fault, the horizontal stress plays a dominant role. In the deeper strata, the maximum horizontal principal stress, the minimum horizontal principal stress and the lateral pressure coefficient exhibit no obvious change with distance from the fault. 3) According to the inversion of the *in-situ* stress field and the stress in the tunnel site, the *in-situ* stress in the tunnel barrel is affected by the depth and the fault. The *in-situ* stress is higher at greater depths. The *in-situ* stress is partially released at the fault so that the *in-situ* stress is relatively low, and the degree of stress decline at different faults is different. 4) Tunnel rockbursts tend to occur in surrounding rock sections with high stress, which are usually located in the middle of a rock mass between two faults. Large deformation mainly occurs in the fault and its influence zone.

Keywords: fault zone, *in-situ* stress, underground engineering, rockburst, large deformation

INTRODUCTION

Regarding underground engineering construction, the *in-situ* stress field environment affects the mechanical response of the surrounding rock during excavation, so it is necessary to investigate the *in-situ* stress characteristics of the surrounding rock (Lu et al., 2012; Ai et al., 2020). As the number of deeply buried long tunnels in complex and dangerous mountain areas increases, the difficulties tunnel construction faced, such as rockburst and large deformation, are becoming more prominent, which is closely related to the geological environment (Jia et al., 2020; Lin et al., 2017). For example, the tunnel of the Shiman expressway had serious deformation, which was related to the tectonic effect of the Yunxi-Yunxian fault zone in the crossing area (Luo et al., 2006). The geological structure of Pajares in the Cantabrian Mountains in northern Spain or the geomechanical anisotropy of the rock contact zone with its strength differences affected the high-speed railway tunnels in this area, resulting in significant deformation along some areas of four tunnels during excavation (Hijazo and de Vallejo, 2012). Gaoligong Mountain is located in the southern Hengduan Mountain near the collision suture zone between the Indian plate and Eurasian plate. Due to large topographic fluctuations, complex structures and strong activity, tunnel construction was facing many problems (Yu et al., 2017). The rock mass along a tunnel of the Iranian water conveyance system located in the contact zone between the Iranian plate and the Arabian plate intensified the problems related to tunnel excavation and compression due to strong joints and faults in the surrounding rock (Ajalloeian et al., 2017). The *in-situ* stress field will be disturbed when the tunnel crosses the fault zone. And the *in-situ* stress field is an important factor that determines the stress, displacement distribution and failure form of the surrounding rock encountered in underground engineering (Li et al., 2017; Zhang et al., 2019). Therefore, studying the influence of faults on the *in-situ* stress field is helpful to analyze the geological information and risk of tunnel rock mass instability, to ensure the safe design and construction of underground engineering.

Many scholars (Li and Miao, 2016; Guo et al., 2017; Cao et al., 2018; Zhao et al., 2019; Qiao, 2021; Zhang, 2021) have analyzed the characteristics of *in-situ* stress based on measured data or stress field inversion results, and some scholars (Zoback and Roller, 1979; Bell and Babcock, 1986; Stephansson and Angman, 1986; Martin, 1990; Aleksandrowski et al., 1992; Lei and Chen, 2011; Li et al., 2012; Ren et al., 2019; Pham et al., 2020; Yang, 2020) have studied the influence of fault zones on *in-situ* stress. Ren Huiliang et al. studied the influence of composite structures, including faults and folds, on the distribution patterns of the *in-situ* stress field (Ren et al., 2019). Yang Yalun investigated the influence of fault structure on the *in-situ* stress field by establishing a small-scale model of a fault area (Yang, 2020). Aleksandrowski et al. found that in a NE-trending normal fault, the stress orientation on one of the two sides of the fault was consistent with the regional stress orientation, while the maximum horizontal principal stress of the other plate was deflected by nearly 90°. Near a fault in Canada, the maximum



FIGURE 1 | Topographic map of the tunnel site.

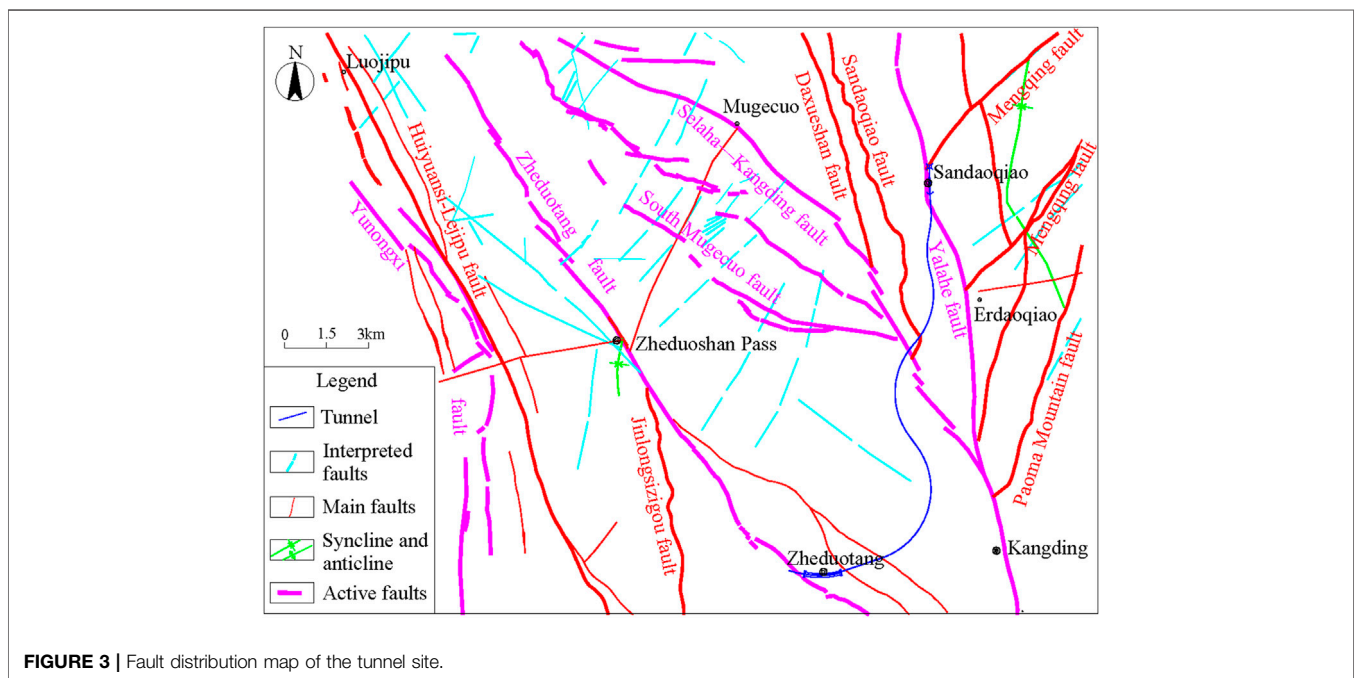
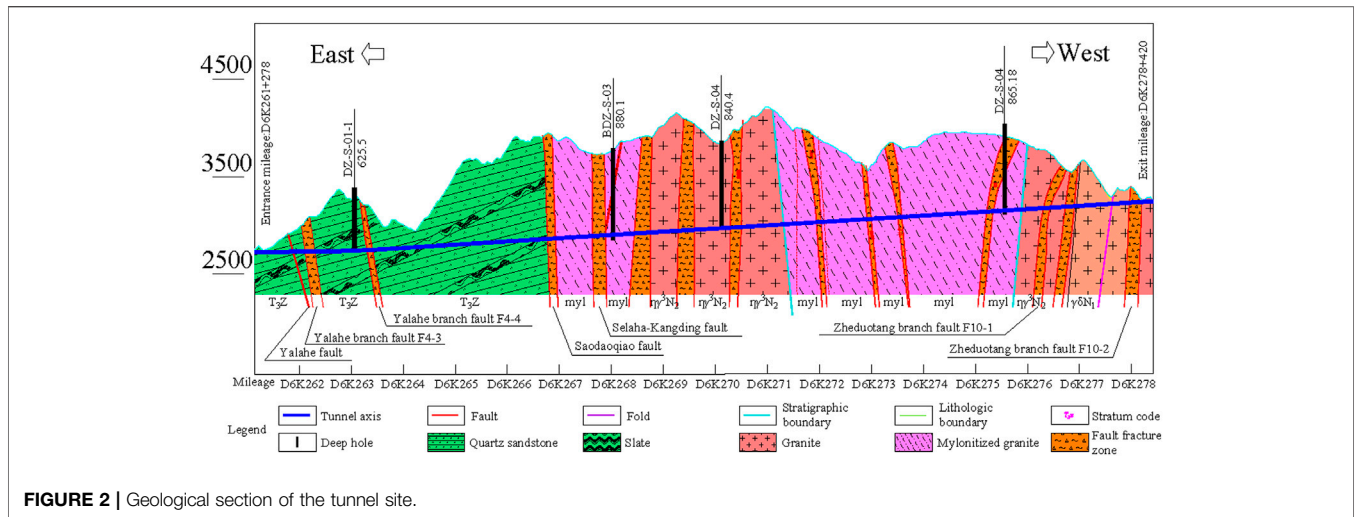
deflection was measured to be more than 45° from the direction of a regional principal stress (Aleksandrowski et al., 1992). Lei Xianqun et al. applied the discontinuous contact model to study the impact of faults on crustal stress and concluded that the fault zone had a high shear stress, while the maximum horizontal principal stress in the nearby local area was weakened to a certain extent (Lei and Chen, 2011). Zoback found that the horizontal principal stress increases with increasing depth and increases gradually with increasing distance from the fault (Zoback and Roller, 1979). The maximum principal stress and shear stress near a fault are low. With the gradual increase in the distance between a measuring point and a fault, the two types of stress values increase significantly. Some scholars also found that the change in the maximum horizontal principal stress near a fault zone was not continuous. There have been many studies on the distribution characteristics of the *in-situ* stress field. However, because a fault is usually simplified into a homogeneous rock mass in simulation and *in-situ* stress data measured across faults are relatively scarce, the influence of a fault zone on the local *in-situ* stress is still not particularly clear (Chen, 2022). Therefore, it is of great significance to further study the influence of fault zones on the *in-situ* stress field.

Taking a tunnel in the Xianshuihe fault zone as the research object, this paper analyzes the influence of the Xianshuihe fault zone on the local *in-situ* stress field based on measured *in-situ* stress data. Combined with the three-dimensional inversion of the *in-situ* stress field, the distribution characteristics of the *in-situ* stress along the tunnel are studied. The prediction and analysis of tunnel rockburst and large deformation are carried out, which provides a reference for the design of engineering construction and safety plans.

GEOLOGICAL SETTING

Topography

The tunnel is located on the southwestern margin of the transition between the Sichuan Basin and the Tibetan Plateau. The Minjiang River, Dadu River and other river systems with severe cutting result in large topographic height differences and complex landforms. The surface elevation of the region is



2,715–4,225 m, and the exogenous forces are mainly glacial water erosion and freezing and thawing, accompanied by biological weathering. The tunnel site topography is a typical plateau landform as shown in **Figure 1**.

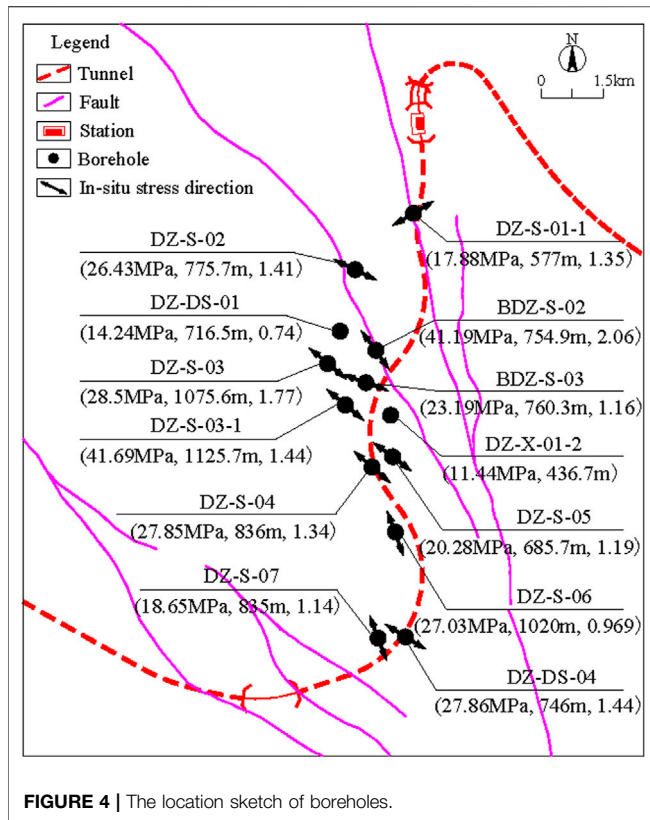
Formation Lithology

As shown in **Figure 2**, the strata exposed in the tunnel site mainly consist of Quaternary Holocene sediments: the colluvial layer is coarse breccia soil, gravel soil and block rock soil, the alluvial-diluvial layer is silty clay (breccia), fine pebble soil, pebble soil and drift rock soil, and the slope residual layer is silty clay (breccia), coarse (fine) breccia soil and gravel soil (breccia). The underlying bedrock is metamorphic quartz sandstone with slate of the

Upper Triassic Zagunao Formation. The strata in this area also include granodiorite, fine-grained biotite monzogranite and mylonitized granite.

Geological Structure

The tunnel is located west of the junction between the Yangtze block and the Qiangtang-Sanjiang orogenic system, the Kang-Yunnan basement complex belt of the Yangtze block in the east, and the Yajiang remnant basin of the Qiangtang-Sanjiang orogenic system in the west. The tunnel site is located in the southeastern margin of the Songpan-Ganzi orogenic belt, where folds and faults are well developed and predominantly trend NNE, followed by NS and NNW. In terms of first-order structure, the tunnel site is located at the junction of the Sichuan-Yunnan



syncline, Kang-Yunnan syncline and Longmenshan fold belt of the Songpan-Ganzi fold belt on the western margin of the Yangtze platform, adjacent to the Kang-Yunnan axis to the west, the Longmenshan structural belt to the north, the Western Sichuan platform depression of the Sichuan platform depression to the east, and the Liangshan depression fold bundle to the south. In terms of secondary structure, it is located in the Xianshuihe structural belt. The orientations of the structures near the tunnel site are mainly $N20^{\circ}\sim 30^{\circ}W$, which is consistent with the strike of the Xianshuihe fault zone, as shown in Figure 3. The faults developed around the tunnel and were greatly influenced by the Yalaha fault and Selaha-Kangding fault. The Yalaha fault is near the entrance end of the tunnel, and the rocks at the entrance end of the tunnel have been seriously crushed. The rocks are obviously cataclastic, and joints have developed. The tunnel site is dominated by NW-trending faults, followed by NE-trending faults (interpreted faults).

IN-SITU STRESS MEASUREMENTS AND MAIN CHARACTERISTICS

The In-Situ Stress Testing Method

The hydraulic fracturing method, one of the recommended methods for determining rock stress issued by the ISRM Commission on Testing Methods in 1987, was used to measure the *in-situ* stress of deep holes near the tunnel. The test section of each borehole was determined according to the test

requirements and the actual situation of the corresponding test hole, and the straddle packer system was used for the test. Water was injected into the test section through the drill pipe, and the water injection pressure was recorded through the wireless pressure sensor placed on the surface. The measured record curve was analyzed to obtain the characteristic pressure parameters and the minimum principal stress of the formation. Then, according to the corresponding theoretical formula, the magnitude of the maximum horizontal principal stress at the measuring point and the rock mechanical parameters such as the hydraulic fracturing tensile strength of the rock were calculated. The baseline orientation and fracturing crack orientation can be obtained through the impression tool and orientation tool, and the orientation of the maximum horizontal principal stress can be further calculated. Thirteen boreholes were tested for *in-situ* stress by the hydraulic fracturing method. Their positions are shown in Figure 4, and the measurements are shown in Table 1. Based on the measured data, the *in-situ* stress magnitude, maximum principal stress direction and lateral pressure coefficient of the tunnel section were analyzed.

The In-Situ Stress Value

Table 1 shows that the maximum horizontal principal stress (S_H) measured in the Xianshuihe fault zone ranges from 6.18 to 41.69 MPa, the minimum horizontal principal stress (S_h) ranges from 4.37 to 29.84 MPa, and the vertical stress (S_V) ranges from 7.41 to 35.85 MPa within the hole depth range of 279.5–1,353 m. According to the measured borehole stress data, a scatter diagram of the stress value and depth is shown in Figure 5. In general, the *in-situ* stress increases gradually with increasing depth. Through linear fitting, the formula of the principal stress gradient can be obtained:

$$S_H = 0.0533H - 14.6247 \quad (1)$$

$$S_h = 0.0382H - 10.2708 \quad (2)$$

where H represents the depth, m. The maximum and minimum horizontal principal stress gradients are approximately 5.33 MPa/100 m and 3.82 MPa/100 m, respectively, and the S_h gradient is less than 2.66 MPa/100 m of the vertical stress gradient.

Maximum Principal Stress Direction

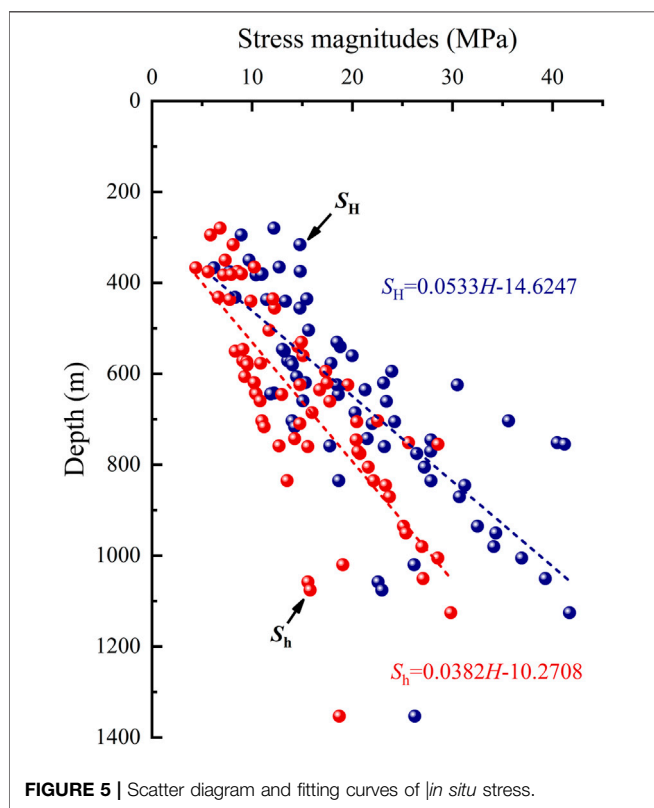
Figure 6 shows the relationship between the principal stress directions and depth of the measured holes near this tunnel, and the dominant orientation of the maximum horizontal principal stress is NW. The direction of the maximum horizontal principal stress is mainly $N40^{\circ}W \sim N75^{\circ}W$, and the azimuth angle of the maximum horizontal principal stress becomes more concentrated in distribution with increasing burial depth. Faults in the tunnel site mainly strike NW, and the direction of the maximum horizontal principal stress is consistent with the strike of fault.

Lateral Pressure Coefficient

The lateral pressure coefficient k is used to study the distribution law of horizontal stress. The closer this value is to 1, the closer the stress state is to hydrostatic. The larger the value is, the more

TABLE 1 | Statistical table of *in-situ* stress and rock types in the tunnel site of the Xianshuihe fault zone.

Borehole number	Test depth range (m)	Maximum horizontal principal stress (MPa)	Minimum horizontal principal stress value (MPa)	Formation lithology	Direction of maximum horizontal principal stress
DZ-S-01-1	571.40–577.00	13.55–17.88	9.07–10.84	Sand slate	N59°E
DZ-S-02	775.00–1005.00	26.43–36.91	20.76–28.53	Granite	N56°W–N68°W
DZ-DS-01	642.50–716.50	11.85–14.24	10.33–11.19	Granite	Not measured
BDZ-S-02	594.6–754.9	23.94–41.19	17.35–28.55	Fault breccia	N24.3°W–N40.4°W
DZ-S-03	279.5–1353	12.17–26.24	6.8–18.71	Fault breccia	N30.5°W–N70.7°W
BDZ-S-03	645.6–760.3	18.6–23.19	12.95–15.56	Granite	N70°E
DZ-S-03-1	560.0–1125.0	19.99–41.69	15.08–29.84	Granite	N55°W–N63°W
DZ-S-05	380.0–685.0	10.99–20.28	8.94–15.98	Limestone	N53°W–N65°W
DZ-S-04	455.0–835.0	14.78–27.85	12.23–22.12	Limestone	N49°W–N57°W
DZ-S-06	550.5–1020	13.22–26.18	8.31–19.05	Fault breccia	N2.8°W–N39.7°W
DZ-DS-04	365.0–745.0	12.70–27.86	10.22–20.39	Limestone	N58°W–N69°W
DZ-S-07	294.5–835.0	8.91–18.65	5.85–13.49	Crushed rock	N20.7°W–N71.6°W
DZ-X-01-2	350–436.7	9.7–11.44	7.31–7.91	Mylonitic granite	N31°E–N70°E

**FIGURE 5** | Scatter diagram and fitting curves of *in situ* stress.

dominant the horizontal tectonic force. The lateral pressure coefficient k is also expressed by the ratio of the average value of the two horizontal stresses to the vertical stress, and the calculation formula is as follows:

$$k = \frac{(S_H + S_h)}{(2S_V)} \quad (3)$$

According to **Formula (3)**, the lateral pressure coefficients of each measured hole are shown in **Table 2**. The lateral pressure coefficients range from 0.560 to 1.744. The lateral pressure

coefficients of holes DZ-S-02, BDZ-S-02, DZ-S-03-1, DZ-S-05, DZ-S-04 and DZ-DS-S-04 are greater than 1, and the *in-situ* stress is $S_H > S_h > S_V$, indicating that horizontal tectonic activity is dominant in the vicinity of these holes. The lateral pressure coefficients of holes DZ-DS-01, BDZ-S-03, DZ-S-06, DZ-S-07 and DZ-X-01-2 are mainly less than 1, and the *in-situ* stress mainly shows $S_H > S_V > S_h$, indicating that the self-weight of the rock plays a dominant role in determining the stress state near these holes.

INFLUENCE OF THE FAULT ZONE ON THE STRESS DISTRIBUTION OF THE TUNNEL SITE

The Xianshuihe fault zone mainly experienced two periods of tectonic stress field activity (Xie et al., 1995). At present, the Xianshuihe horizontal fault zone is characterized by sinistral strike-slip movement, and its activity may affect the local *in-situ* stress field.

Influence Characteristics of the Fault Zone on the *In-Situ* Stress

To understand the influence of the Xianshuihe fault zone on the *in-situ* stress as a whole, the boreholes near a tunnel are divided into four categories according to the distance perpendicular to the nearest fault strike: 0–500 m, 500–1,000 m, 1,000–1,500 m and 1,500–2,000 m. The relationships between the measured maximum horizontal principal stress, minimum horizontal principal stress, maximum principal stress direction and the burial depth and distance to the fault are shown in **Figures 7A,B,C**, respectively. As shown in **Figures 7A,B**, the maximum horizontal principal stress and the minimum horizontal principal stress linearly increase with increasing burial depth. Regardless of the distance from the fault, the rate of increase in the maximum horizontal principal stress with burial depth is greater than that in the minimum horizontal

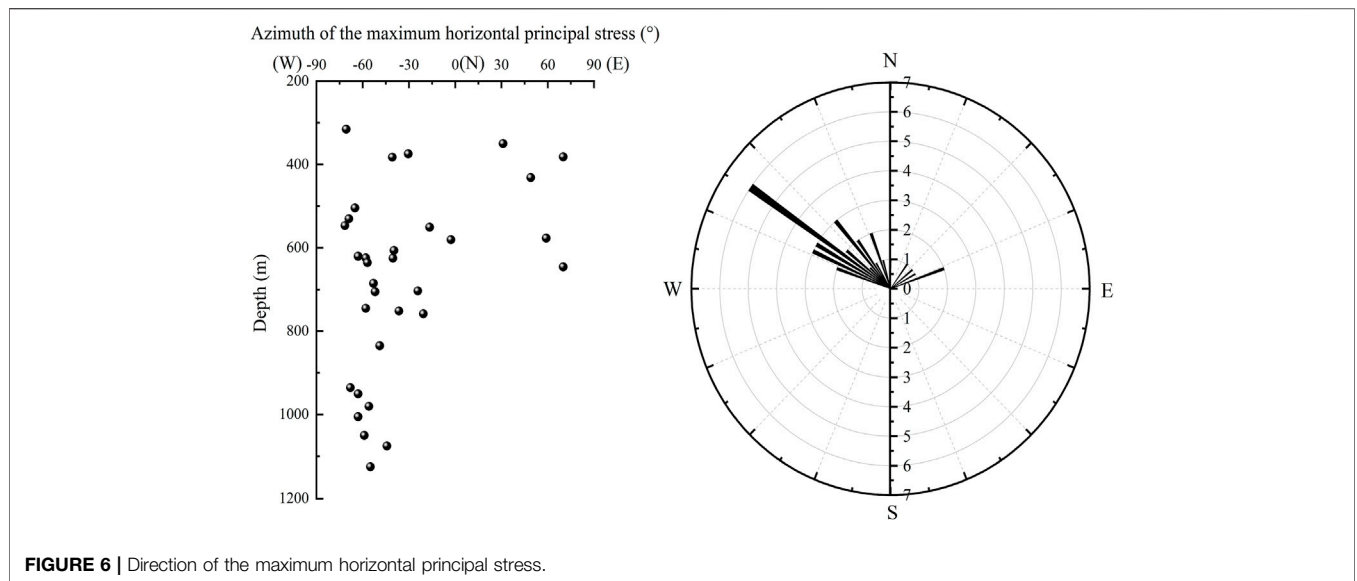


FIGURE 6 | Direction of the maximum horizontal principal stress.

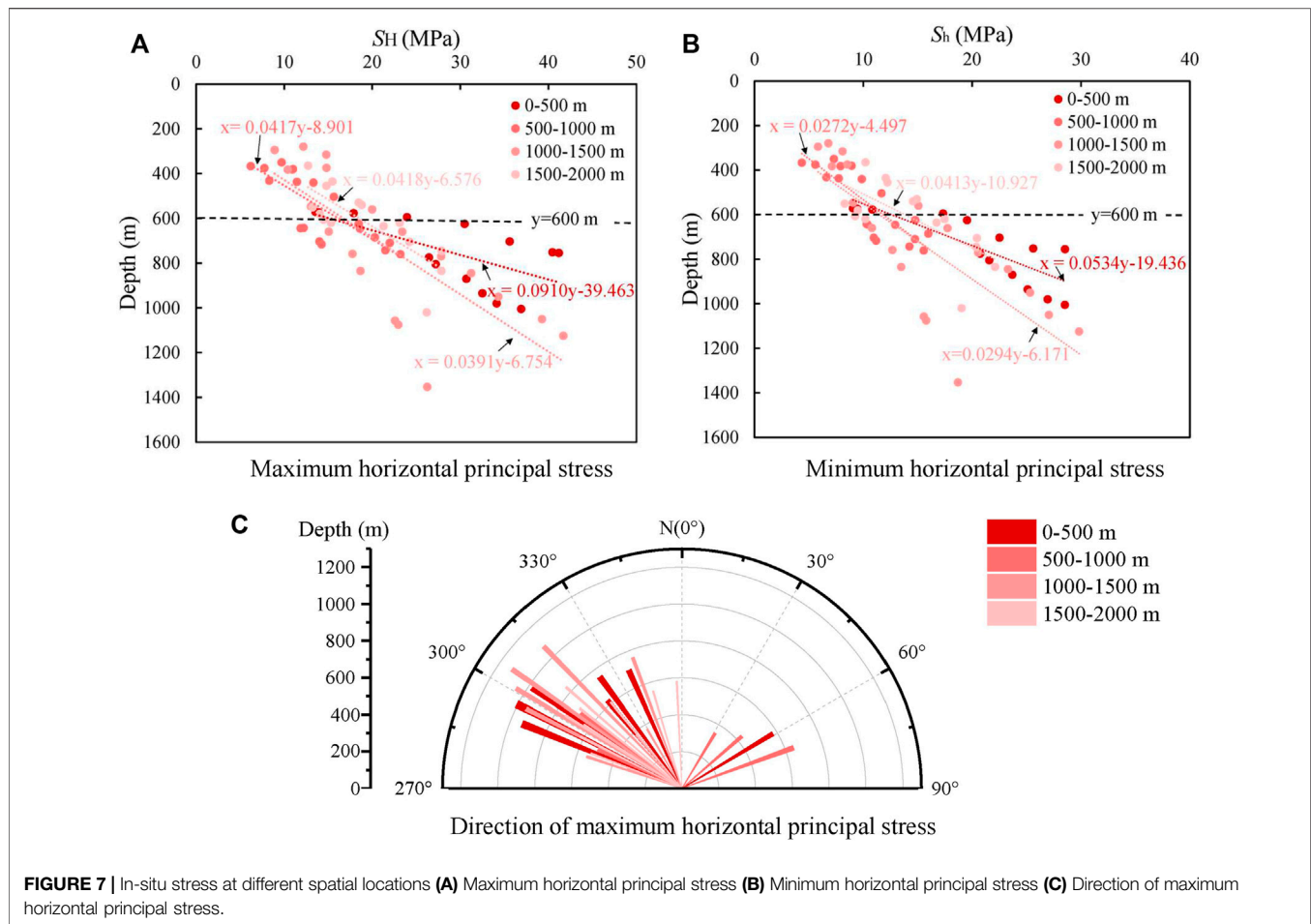
TABLE 2 | Lateral pressure coefficients of different boreholes.

Hole	Lateral pressure coefficient	Lateral pressure coefficient
DZ-S-01-1	0.860~1.082	$S_H > S_v > S_h, S_H > S_h > S_v$
DZ-S-02	1.165~1.252	$S_H > S_h > S_v$
DZ-DS-01	0.646~0.664	$S_H > S_v > S_h$
BDZ-S-02	1.309~1.743	$S_H > S_h > S_v$
DZ-S-03	0.679~1.368	$S_H > S_v > S_h, S_H > S_h > S_v$
BDZ-S-03	0.918~0.988	$S_H > S_v > S_h$
DZ-S-03-1	1.199~1.241	$S_H > S_h > S_v$
DZ-S-05	1.008~1.042	$S_H > S_h > S_v$
DZ-S-04	1.141~1.218	$S_H > S_h > S_v$
DZ-S-06	0.737~0.836	$S_H > S_v > S_h$
DZ-DS-S-04	1.207~1.259	$S_H > S_h > S_v$
DZ-S-07	0.726~0.946	$S_H > S_v > S_h$
DZ-X-01-2	0.559~0.958	$S_H > S_v > S_h$

principal stress. In addition, when the burial depth is less than 600 m, the farther the borehole is from the fault, the greater the measured maximum horizontal principal stress and minimum horizontal principal stress. When the burial depth is greater than 600 m, the variations in the maximum horizontal principal stress and minimum horizontal principal stress with increasing distance to the fault are not consistent. Therefore, the fault has a significant differential impact on the *in-situ* stress of the shallow stratum. The fastest rates of increase in the maximum horizontal principal stress and minimum horizontal principal stress, which are 0.0910 MPa/m and 0.0534 MPa/m, respectively, are observed at the boreholes less than 500 m from the fault. When the distance from a borehole to the fault is greater than 500 m, the trend of the rate of increase in maximum horizontal principal stress with the distance from the borehole to the fault is not obvious, and the rate of increase in the minimum horizontal principal stress increases slightly with increasing distance from the fault. As shown in **Figure 7C**, when a borehole is less than

1,000 m from the fault, the direction of the maximum principal stress of the borehole is different from the dominant NW direction of the maximum principal stress in the area, instead showing a NE direction. The *in-situ* stress direction near the fault is complex and may be deflected under the influence of the fault.

To investigate the distribution characteristics of *in-situ* stress in the control area of a single fault in the Xianshuihe fault zone, the measured *in-situ* stress values of boreholes perpendicular to the strike of the Selaha-Kangding fault are selected for analysis. Because the factors affecting the *in-situ* stress are mainly the burial depth and fault, the horizontal principal stress of the same burial depth is selected for comparison between different boreholes to eliminate the influence of burial depth. Considering that there are some differences in the range of the measured sections of the boreholes, boreholes with the same depths are selected for analysis. According to the above analysis, the *in-situ* stress obeys different laws in deep and shallow strata. Therefore, for the borehole measured sections selected, burial depth ranges of less than 600 m and more than 600 m are selected for comparison (namely, burial depths of 450 and 750 m). Among them, boreholes DZ-X-01-2, BDZ-S-03, DZ-S-03, DZ-S-04 and DZ-S-05 are selected for the 450 m burial depth, and boreholes BDZ-S-02, DZ-S-02, DZ-DS-01, DZ-S-03-1 and DZ-S-06 are selected for the 750 m burial depth. The stress values of each burial depth are obtained based on the approximate linear relationship between the measured stress value and the burial depth. The relationships between the maximum horizontal principal stress, the minimum horizontal principal stress, the lateral pressure coefficient and the distance from the borehole to the fault are shown in **Figure 8**. As shown in **Figure 8A**, for the boreholes near the Selaha-Kangding fault, when the burial depth is 450 m, the overall maximum horizontal principal stress and minimum horizontal principal stress increase with increasing distance from the fault. The maximum horizontal principal stress and the minimum horizontal principal stress of the borehole



farthest from the fault increased by nearly 47 and 66%, respectively, compared with the maximum horizontal principal stress and the minimum horizontal principal stress of the borehole nearest to the fault. **Figure 8B** shows that when the borehole is close to the fault, k is less than 1, which means that the geostatic stress is dominant; however, when the fault distance is greater than 600 m, k is greater than 1, which means that the tectonic stress is dominant. This may be because in the shallow area, the tectonic influence is weakened due to the deterioration of rock mass properties near the fault, so the horizontal stress is reduced more. As shown in **Figures 8C,D**, when the burial depth is 750 m, the variation pattern of the maximum horizontal principal stress, minimum horizontal principal stress and lateral pressure coefficient with the distance from the borehole to the fault is not significant, which may be due to the greater influence of gravity of the rock mass in the deep area and the weakening of tectonic influence, so the change in horizontal stress is not obvious.

Distribution Characteristics of the *In-Situ* Stress at the Tunnel Barrel

To ensure the safety of tunnel construction, it is necessary to determine the *in-situ* stress distribution along the tunnel.

Therefore, based on the inversion of the *in-situ* stress field at the tunnel site, the contour map of the maximum principal stress of the section where a tunnel is located and the line map of the maximum principal stress at the tunnel depth are extracted, as shown in **Figure 9**. It can be seen from this figure that the maximum horizontal principal stress of the tunnel is 3~44 MPa, and the *in-situ* stress of the entrance and exit of the tunnel is low, while the *in-situ* stress in the surrounding rock of the tunnel barrel is high. The maximum horizontal principal stress of the tunnel barrel is affected by the depth and fault. The maximum horizontal principal stress increases with increasing depth, while the *in-situ* stress release at the fault leads to a decrease in the *in-situ* stress, which corresponds to an area of lower *in-situ* stress at the fault on the contour map of the maximum horizontal principal stress. However, the *in-situ* stress increases away from the fault, and there is usually a maximum *in-situ* stress in the tunnel segment between two faults due to the dual influence of burial depth and fault. For example, the highest maximum horizontal principal stress between the Yalaha fault and the Sandaoqiao fault is 34 MPa, which is approximately three times the maximum horizontal principal stress at the Yalaha fault and the Sandaoqiao fault. The highest maximum horizontal principal stress between the Sandaoqiao fault and the Selaha-Kangding fault is approximately 28 MPa, which is approximately three times the maximum horizontal principal stress value at the Sandaoqiao fault and approximately twice the maximum horizontal principal stress

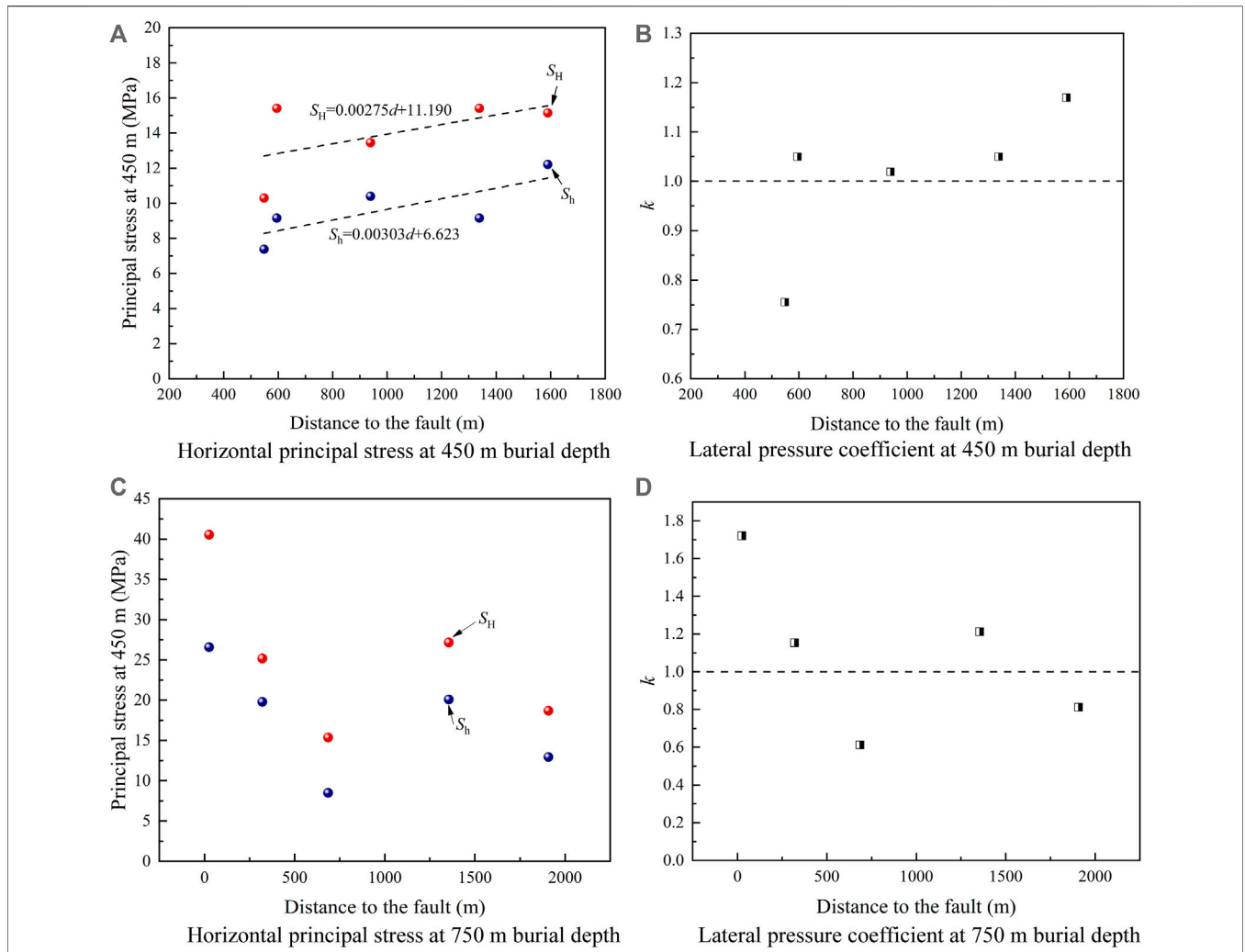


FIGURE 8 | The relationship between horizontal principal stress and lateral pressure coefficient of borehole and the distance to the fault (d represents the distance from borehole to fault) **(A)** Horizontal principal stress at 450 m burial depth **(B)** Lateral pressure coefficient at 450 m burial depth **(C)** Horizontal principal stress at 750 m burial depth **(D)** Lateral pressure coefficient at 750 m burial depth.

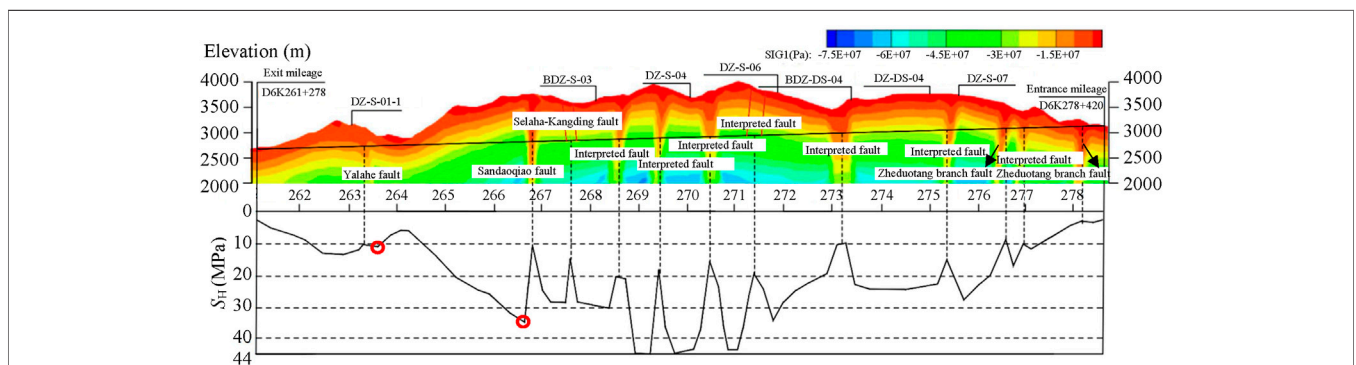


FIGURE 9 | The contour map and line chart of the maximum horizontal principal stress of a tunnel.

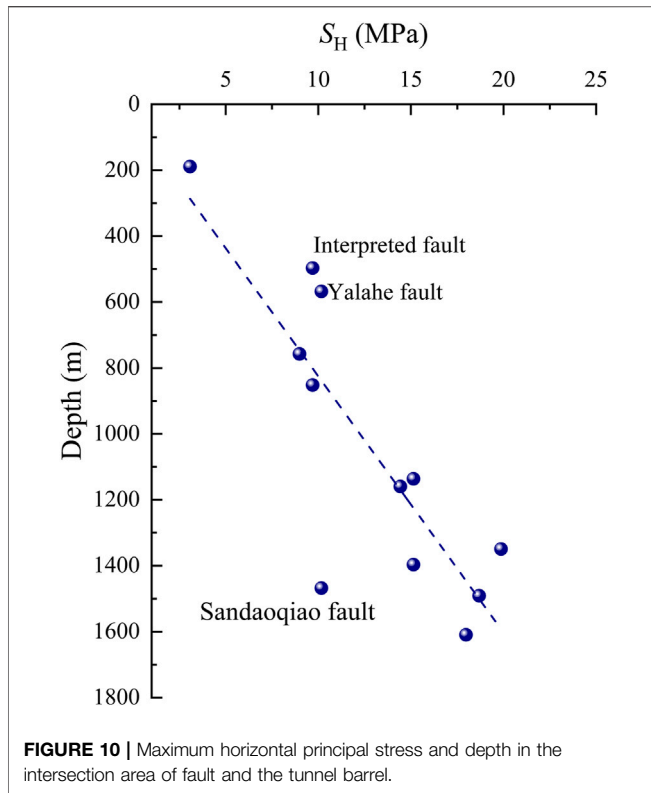


FIGURE 10 | Maximum horizontal principal stress and depth in the intersection area of fault and the tunnel barrel.

value at the Selaha-Kangding fault. From the variation in the maximum horizontal principal stress between the Sandaoqiao fault and the Selaha-Kangding fault, it is obvious that the variation in the maximum horizontal principal stress of the rock mass between the two faults is roughly the same as that of the burial depth of the tunnel barrel. This phenomenon indicates that the maximum horizontal principal stress of the middle segment is mainly controlled by depth. Moreover, there is stress concentration near the fault due to tectonic influence.

The relationship between the maximum horizontal principal stress in the intersection area of the tunnel barrel and fault and depth is shown in **Figure 10**. The maximum horizontal principal stress in the intersection area of the tunnel barrel and fault increases roughly with increasing depth, except at the Sandaoqiao fault, Yala River fault and the interpreted fault of mile D6K276 + 996. That is, the depth of the tunnel barrel section of one fault is less than that of the tunnel barrel section of another fault, but the *in-situ* stress value of the former may be greater than that of the latter. For example, the depth of the Sandaoqiao fault (1,467 m) is greater than that of the D6K270 + 565 fault (1,396 m), while the maximum horizontal principal stress value of the former (10 MPa) is less than that of the latter (15 MPa). This indicates that different faults have different effects on the *in-situ* stress.

ENGINEERING EFFECT ANALYSIS

On the whole, the formation of the fault zone reflects the considerable tectonic activity and high *in-situ* stress in this region, and the disturbance of tunnel excavation under high

in-situ stress can easily induce underground engineering disasters such as rockburst and large deformation (Zhang et al., 2021). Many scholars have carried out relevant research (Aydan et al., 1993; Feng et al., 2015; Chen et al., 2020; Feng et al., 2022; Yu et al., 2022). In this section, the prediction of rockburst and large deformation in the tunnel site are carried out.

Rockburst Prediction at the Tunnel Site

The occurrence of rockburst is affected by many factors, so these factors should be comprehensively considered to establish their prediction criteria. In this paper, the strength-stress ratio method is used for prediction and combined with the results of the geological analysis method. The geological analysis method mainly aims at macroscale prediction, taking geological exploration data as the basis and similar engineering data as the analogy to make a simple macroscale prediction of the research object from the aspects of *in-situ* stress, lithology, hydrology, structural geology and so on. The strength-stress ratio rule is used to establish the quantitative index of rockburst prediction according to the *in-situ* stress and rock mass properties, which is calculated according to the following formula (National Railway Administration of the People Republic of China, 2016):

$$p = \frac{R_c}{\sigma_{max}} \tag{4}$$

where *p* is the rockburst classification index, and the relationship between its value and rockburst classification is shown in **Table 3**. *R_c* is the saturated uniaxial compressive strength of the rock mass; *σ_{max}* is the maximum *in-situ* stress. Although the occurrence of rockburst is caused by stress redistribution due to excavation, the stress redistribution is based on the initial stress of the rock mass. Therefore, the initial maximum horizontal principal stress of the surrounding rock is used in this paper to reflect the relative magnitude of stress redistribution after excavation.

The strength-stress ratio method and geological analysis method were used to analyze and predict a tunnel rockburst. Due to the complex strata, broken rock mass and severe weathering, the surrounding rock is mostly grade IV~V, and only some parts of ηγ³N₂ are grade III. First, it is preliminarily found that the surrounding rocks of grade IV and below do not have the conditions of rockburst, so rockburst is not considered, and only the possibility of rockburst occurring in the surrounding rocks of grade III and above is considered, so the rockburst discrimination and prediction analysis is

TABLE 3 | Rockburst grade of hard rock section (National Railway Administration of the People Republic of China, 2016).

Rockburst grade	Strength-stress ratio of surrounding rock (<i>R_c</i> / <i>σ_{max}</i>)
Light	4~7
Moderate	2~4
Severe	<2

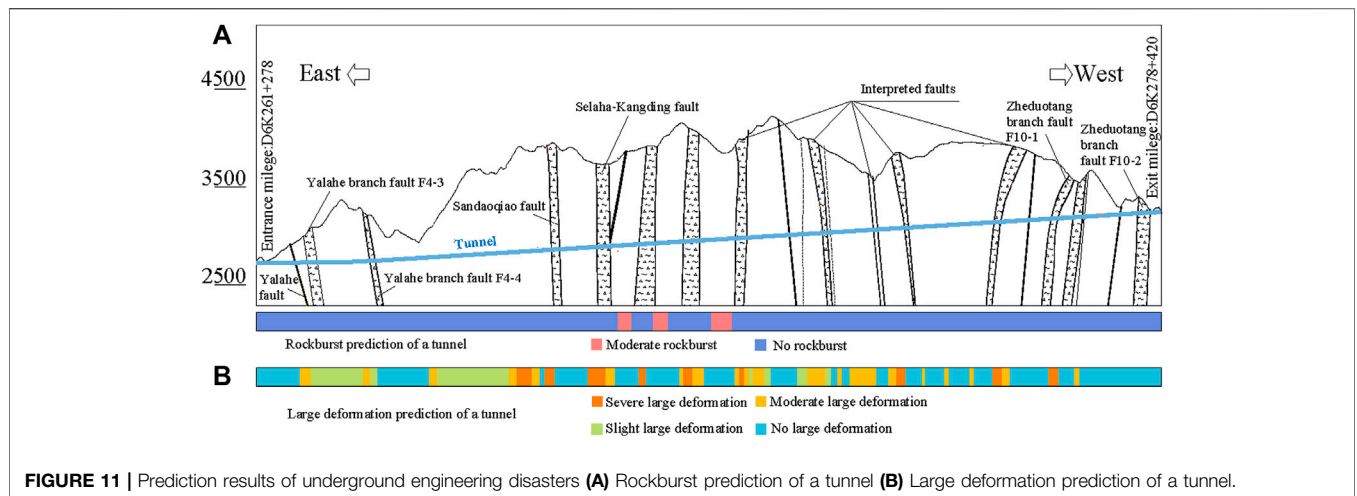


FIGURE 11 | Prediction results of underground engineering disasters (A) Rockburst prediction of a tunnel (B) Large deformation prediction of a tunnel.

TABLE 4 | Large deformation grade (National Railway Administration of the People Republic of China, 2016).

Deformation grade of soft rock with high in-situ stress	Strength-stress ratio of surrounding rock (R_b/σ_{max})	The deformation trend
I	0.25–0.5	Light
II	0.15–0.25	Moderate
III	<0.15	Severe

carried out only for the surrounding rocks of grade III. According to the rock burst prediction results of a tunnel obtained by the strength stress ratio method and geological analysis method (as shown in Figure 11A), rockburst occurs mainly in grade III surrounding rock of $\eta\gamma^3N_2$, where the rock mass strength is higher, and the section is mainly in the middle of a rock mass between two adjacent faults, so the maximum principal stress value is relatively high (greater than 30 MPa). The tunnel is mainly subject to moderate rockburst, and the length of the tunnel with moderate rockburst is 980 m.

Prediction of Large Deformation at the Tunnel Site

The classification index for large deformation prediction of soft rock segments is calculated according to the strength-stress ratio formula (5)(National Railway Administration of the People Republic of China, 2016):

$$q = \frac{R_b}{\sigma_{max}} \tag{5}$$

where q is the large deformation classification index, and its value and corresponding large deformation classification are shown in Table 4. R_b is the strength of the surrounding rock mass; σ_{max} is the maximum *in-situ* stress.

According to the numerical results of the tunnel axis stress corresponding to the mileage section of the *in-situ* stress simulation and geological prospecting section division, the

identification and division of the large deformation of the surrounding rock were carried out, and the prediction results of large deformation were obtained (as shown in Figure 11B). The results of large tunnel deformation include slight large deformation, moderate large deformation, and severe large deformation, and most of them occur in fault zones or affected areas of fault zones. Although the *in-situ* stress at the fault is relatively low, the rock strength here is also low, so large deformation easily occurs. In the statistical range, the length of the section with severe large deformation is 1900 m, accounting for 11% of the total length of the tunnel, and almost all of them occur at the fault. In these sections, the *in-situ* stress is higher than 12 MPa, mostly at the moderate stress level. Due to the low strength of the surrounding rock, the final strength-stress ratio is low. The moderately large deformation section is 3,170 m, accounting for 18.35% of the total length of the tunnel. Most of these sections are faults or fault-affected areas. There are two situations: one is that the *in-situ* stress value is equal to or even slightly lower than the *in-situ* stress value of the section with severe large deformation, and the strength of the surrounding rock is slightly higher than that of the section with severe large deformation; the other is that the *in-situ* stress value of the $\eta\gamma^3N_2$ stratum is very high (all greater than 40 MPa), and the strength of the surrounding rock is relatively high. In both cases, moderate deformation is more likely to occur. The section with slightly large deformation is 2,940 m, accounting for 17.02% of the total length of the tunnel. Most of these

sections are affected areas of fault zones or T_3z and myl strata. The *in-situ* stress level of this section is relatively low, mostly below 20 MPa, and the strength of the surrounding rock is relatively high.

CONCLUSION

The *in-situ* stress of a tunnel site in the Xianshuihe fault zone is analyzed, and the following conclusions are drawn:

- 1) Regarding the overall situation of the Xianshuihe fault zone, the fault mainly affects the maximum horizontal principal stress and the minimum horizontal principal stress in the shallow stratum. The *in-situ* stress near the fault is greatly affected, resulting in a deviation in the direction of the maximum principal stress from the direction of the regional dominant principal stress. In the shallow area near the Selaha-Kangding fault, the maximum horizontal principal stress, minimum horizontal principal stress and lateral pressure coefficient of the borehole increase with increasing distance from the fault. Farther than 600 m from the fault, the horizontal stress is greatest. In the deeper area, the maximum horizontal principal stress, the minimum horizontal principal stress and the lateral pressure coefficient exhibit no obvious change with increasing distance from the fault.
- 2) According to the inversion of the *in-situ* stress field in the studied tunnel site and the stress in the tunnel, the maximum principal stress in the axial direction of a tunnel is 3~44 MPa, the *in-situ* stress at the entrance and exit of the tunnel is low, and the *in-situ* stress at the tunnel barrel is high. The *in-situ* stress around the tunnel barrel is affected not only by the burial depth but also by the fault. The *in-situ* stress at greater burial depths is high, and the *in-situ* stress at the fault has been released to a certain extent. The *in-situ* stress is relatively low, and the degree of stress decline at different faults is different.
- 3) The rockburst prediction results for the tunnel are obtained by the comprehensive strength-stress ratio method and

geological analysis method. The prediction results are as follows: the length of the moderate rockburst risk is 980 m, accounting for 5.67%, which tends to coincide with the rock section with high stress located in the middle of a rock mass between two faults. The large deformation grade of the tunnel is obtained by the strength-stress ratio method, which mainly indicates in slight large deformation, moderate large deformation, and severe large deformation mainly occurs in the fault and its influence zone. The length of slight large deformation is 2,940 m, accounting for 17.02%. The length of moderate large deformation is 3,170 m, accounting for 18.35%. The length of severe large deformation is 1900 m, accounting for 11%.

DATA AVAILABILITY STATEMENT

The original contributions presented in the study are included in the article/Supplementary Material, further inquiries can be directed to the corresponding authors.

AUTHOR CONTRIBUTIONS

DY mainly participated in the field work and formed the idea of the article. LZ and XL wrote the first draft of the manuscript. All authors contributed to manuscript revision, read, and approved the submitted version.

FUNDING

This study was funded by the research project of China Railway Eryuan Engineering Group Company, Ltd. (Grant Nos. KSNQ200002, KDNQ213043, KSNQ213010, and KDNQ201004).

REFERENCES

- Ajalloeian, R., Moghaddam, B., and Azimian, A. (2017). Prediction of Rock Mass Squeezing of T4 Tunnel in Iran. *Geotech Geol. Eng.* 35 (2), 747–763. doi:10.1007/s10706-016-0139-y
- Ai, T., Wu, S. Y., Zhang, R., Gao, M. Z., Zhou, J. E., Xie, J., et al. (2021). Changes in the Structure and Mechanical Properties of a Typical Coal Induced by Water Immersion. *Int. J. Rock Mech. Min.* 138. doi:10.1016/j.ijrmms.2020.104597
- Aleksandrowski, P., Inderhaug, O. H., and Knapstad, B. (1992). "Tectonic Structures and Wellbore Breakout Orientation," in Proceedings of the 33rd United-States Symp on Rock Mechanics, Rotterdam, Netherlands, June 1992, 29–37.
- Aydan, O., Akagi, T., and Kawamoto, T. (1993). The Squeezing Potential of Rocks Around Tunnels; Theory and Prediction. *Rock Mech. Rock Engng* 26 (2), 137–163. doi:10.1007/bf01023620
- Bell, J. S., and Babcock, E. A. (1986). The Stress Regime of the Western Canadian Basin and Implications for Hydrocarbon Production. *Bull. Can. Pet. Geology* 34 (3), 364–378.
- Cao, P., Li, K., Li, C. J., and Zhang, L. D. (2018). Back-Calculation of Ground Stress Field and Rockburst Analysis for Wunvfeng Tunnel. *Mod. tunnelling Technol.* 55 (05), 45–52. doi:10.13807/j.cnki.mtt.2018.05.006
- Chen, X. Q. (2022). Influence of Fault Fracture Zone on Initial *In-Situ* Stress Field in Tongmai Tunnel of the Sichuan-Tibet Railway. *Earth Sci.* [Epub ahead of print], 1–9. doi:10.3799/dqkx.2021.263
- Chen, Z., He, C., Yang, W., Guo, W., Li, Z., and Xu, G. (2020). Impacts of Geological Conditions on Instability Causes and Mechanical Behavior of Large-Scale Tunnels: a Case Study from the Sichuan-Tibet Highway, China. *Bull. Eng. Geol. Environ.* 79 (7), 3667–3688. doi:10.1007/s10064-020-01796-w
- Feng, G.-L., Chen, B.-R., Xiao, Y.-X., Jiang, Q., Li, P.-X., Zheng, H., et al. (2022). Microseismic Characteristics of Rockburst Development in Deep TBM Tunnels with Alternating Soft-Hard Strata and Application to Rockburst Warning: A Case Study of the Neelum-Jhelum Hydropower Project. *Tunnelling Underground Space Technol.* 122, 104398. doi:10.1016/j.tust.2022.104398
- Feng, G.-L., Feng, X.-T., Chen, B.-r., Xiao, Y.-X., and Yu, Y. (2015). A Microseismic Method for Dynamic Warning of Rockburst Development Processes in Tunnels. *Rock Mech. Rock Eng.* 48 (5), 2061–2076. doi:10.1007/s00603-014-0689-3

- Guo, C. B., Zhang, Y. S., Jiang, L. W., Shi, J. S., Meng, W., Du, Y. B., et al. (2017). Discussion on the Environmental and Engineering Geological Problems along the Sichuan-Tibet Railway and its Adjacent Area. *GEOSCIENCE* 31 (05), 877–889.
- Hijazo, T., and González de Vallejo, L. I. (2012). *In-situ* Stress Amplification Due to Geological Factors in Tunnels: The Case of Pajares Tunnels, Spain. *Eng. Geology*. 137–138, 13–20. doi:10.1016/j.enggeo.2012.03.007
- Jia, Z. Q., Xie, H. P., Zhang, R., Li, C. B., Wang, M., Gao, M. Z., et al. (2020). Acoustic Emission Characteristics and Damage Evolution of Coal at Different Depths Under Triaxial Compression. *Rock Mech. Rock Eng.* 53 (5), 2063–2076. doi:10.1007/s00603-019-02042-w
- Lei, X. Q., and Chen, Y. P. (2011). Effects of Faults on Crustal Stress Using Discontinuous Model. *J. Cent. South Univ. (Science Technology)* 42 (08), 2379–2386.
- Li, H., Xie, F. R., Wang, H. Z., Dong, Y. K., and Yu, J. J. (2012). Characteristics of *In-Situ* Stress Measurements Near the Fault and Fault Activity in Urumqi City. *Chin. J. Geophys.* 55 (11), 3690–3698. doi:10.6038/j.issn.0001-5733.2012.11.016
- Li, K., Jiang, X. H., Wu, M. J., and Ding, H. (2017). Numerical Reversion of Tunnel Initial Stress Field in Fault Disturbed Zone. *China Civil Eng. J.* 50 (S2), 255–259. doi:10.15951/j.tmgxcb.2017.s2.040
- Li, P., and Miao, S. J. (2016). Analysis of the Characteristics of *In-Situ* Stress Field and Fault Activity in the Coal Mining Area of China. *J. China Coal Soc.* 41 (S2), 319–329. doi:10.13225/j.cnki.jccs.2016.0303
- Lin, D. M., Yuan, R. M., Shang, Y. J., Bao, W. X., Wang, K. Y., Zhang, Z. J., et al. (2017). Deformation and Failure of a Tunnel in the Restraining Bend of a Strike-Slip Fault Zone: An Example from Hengshan Mountain, Shanxi Province, China. *Bull. Eng. Geol. Environ.* 76 (1), 263–274. doi:10.1007/s10064-016-0850-1
- Lu, W. B., Yang, J. H., Yan, P., Chen, M., Zhou, C. B., Luo, Y., et al. (2012). Dynamic Response of Rock Mass Induced by the Transient Release of in-situ Stress. *Int. J. Rock Mech. Min.* 53, 129–141. doi:10.1016/j.ijrmms.2012.05.001
- Luo, X. D., Chen, J. P., Fan, J. H., and Zuo, C. Q. (2006). “Studying on Large Deformation Mechanism of Soft Rock Tunnel Fluctuated by Yunxi-Yunxian Fault,” in Proceedings of the 2nd International Conference on Environmental and Engineering Geophysics, Wuhan, P.R. China, June 4–9, 2006, 927–931.
- Martin, C. D. (1990). Characterizing *In Situ* Stress Domains at the AECL Underground Research Laboratory. *Can. Geotech. J.* 27 (5), 631–646. doi:10.1139/t90-077
- National Railway Administration of the People Republic of China (2016). *Code for Design of Railway Tunnel*. Beijing: China Railway Publishing House.
- Pham, C., Chang, C., Jang, Y., Kutty, A., and Jeong, J. (2020). Effect of Faults and Rock Physical Properties on *In Situ* Stress within Highly Heterogeneous Carbonate Reservoirs. *J. Pet. Sci. Eng.* 185, 106601. doi:10.1016/j.petrol.2019.106601
- Qiao, Z. B. (2021). Study on Rockburst Intensity Prediction Based on the Characteristics of *In-Situ* Stress Field in Deep Tunnel on Sichuan-Tibet Railway. *Railway Stand. Des.* 65 (02), 89–94+103. doi:10.13238/j.issn.1004-2954.202005120002
- Ren, H. L., Duan, D., and Chen, S. S. (2019). Influence of Composite Structure on the Distribution Characteristics of Geostress. *Mining Res. Develop.* 39 (06), 58–62. doi:10.13827/j.cnki.kyyk.2019.06.012
- Stephansson, O., and Angman, P. (1986). Hydraulic Fracturing Stress Measurements at Forsmark and Stidsvig, Sweden. *Bull. Geol. Soc. Finland* 58 (58), 307–333. doi:10.17741/bgsf/58.1.021
- Xie, F. R., Zhu, J. Z., and Shu, S. B. (1995). Study of Different Stage Quaternary Tectonic Stress Field for the Xianshuihe Fault Zone. *Seismology Geology*. 17 (01), 35–43.
- Yang, Y. L. (2020). Analysis of Geostress Field in the Gong Jue Tunnel of Sichuan-Tibet Railway Project and the Effect of Fractures. Master's thesis. Chengdu: Southwest Jiaotong University.
- Yu, N., Hu, X. Y., Li, J., Zhao, N., Zhou, J., Cai, X. L., et al. (2017). Electrical Structure of the Longling Area in Western Yunnan and its Effect on Route Selection of the Dali-Ruili Railway. *Chin. J. Geophysics-Chinese Edition* 60 (6), 2442–2455. doi:10.6038/cjg20170632
- Yu, Y., Feng, G.-l., Xu, C.-j., Chen, B.-r., Geng, D.-x., and Zhu, B.-t. (2022). Quantitative Threshold of Energy Fractal Dimension for Immediate Rock Burst Warning in Deep Tunnel: A Case Study. *Lithosphere* 2021, 1699273. doi:10.2113/2022/1699273
- Zhang, M., Huang, J., Ju, N. P., Zhang, Y. L., and Zhang, G. Z. (2019). Inverse Analysis on *In-Situ* Stress Field of Super-long and Deep Buried Tunnel in Chuan-Zang Railway. *Chin. J. Underground Space Eng.* 15 (04), 1232–1238+1257.
- Zhang, Y. X. (2021). Characteristics of Current *In-Situ* Stress Field about Sejila Mountain Traffic Corridor. *J. Eng. Geology*. 29 (02), 394–403. doi:10.13544/j.cnki.jeg.2021-0126
- Zhang, A. L., Xie, H. P., Zhang, R., Ren, L., Zhou, J. F., Gao, M. Z., et al. (2021). Dynamic Failure Behavior of Jinping Marble Under Various Preloading Conditions Corresponding to Different Depths. *Int. J. Rock Mech. Min.* 148. doi:10.1016/j.ijrmms.2021.104959
- Zhao, L., Zhang, Z. D., Li, L. M., Wang, P., Meng, J., and Tao, L. (2019). Study on Characteristics of Geostress Field in Qinling Water Conveyance Tunnel of Hanjiang to Weihe River Valley Water Diversion Project and its Inverse Analysis. *Water Resour. Hydropower Eng.* 50, 90–96.
- Zoback, M. D., and Roller, J. C. (1979). Magnitude of Shear Stress on the San Andreas Fault: Implications of a Stress Measurement Profile at Shallow Depth. *Science* 206 (4417), 445–447. doi:10.1126/science.206.4417.445

Conflict of Interest: Author DY, TF, GZ, ZX, ZW, XY and ZL are employed by China Railway Eryuan Engineering Group Co., Ltd.

The remaining authors declare that the research was conducted in the absence of any commercial or financial relationships that could be construed as a potential conflict of interest.

Publisher's Note: All claims expressed in this article are solely those of the authors and do not necessarily represent those of their affiliated organizations, or those of the publisher, the editors and the reviewers. Any product that may be evaluated in this article, or claim that may be made by its manufacturer, is not guaranteed or endorsed by the publisher.

Copyright © 2022 Yuan, Zhang, Liu, Feng, Zhang, Xu, Wang, Yi, Lin, Ren, Zhang and Ren. This is an open-access article distributed under the terms of the Creative Commons Attribution License (CC BY). The use, distribution or reproduction in other forums is permitted, provided the original author(s) and the copyright owner(s) are credited and that the original publication in this journal is cited, in accordance with accepted academic practice. No use, distribution or reproduction is permitted which does not comply with these terms.